



This open access document is posted as a preprint in the Beilstein Archives at <https://doi.org/10.3762/bxiv.2022.91.v1> and is considered to be an early communication for feedback before peer review. Before citing this document, please check if a final, peer-reviewed version has been published.

This document is not formatted, has not undergone copyediting or typesetting, and may contain errors, unsubstantiated scientific claims or preliminary data.

**Preprint Title** Specific absorption rate of randomly oriented magnetic nanoparticles in a static magnetic field

**Authors** Ruslan A. Rytov and Nikolai A. Usov

**Publication Date** 15 Dez. 2022

**Article Type** Full Research Paper

**ORCID® iDs** Ruslan A. Rytov - <https://orcid.org/0000-0002-7963-3673>; Nikolai A. Usov - <https://orcid.org/0000-0002-2061-3467>

License and Terms: This document is copyright 2022 the Author(s); licensee Beilstein-Institut.

This is an open access work under the terms of the Creative Commons Attribution License (<https://creativecommons.org/licenses/by/4.0>). Please note that the reuse, redistribution and reproduction in particular requires that the author(s) and source are credited and that individual graphics may be subject to special legal provisions.

The license is subject to the Beilstein Archives terms and conditions: <https://www.beilstein-archives.org/xiv/terms>.

The definitive version of this work can be found at <https://doi.org/10.3762/bxiv.2022.91.v1>

# Specific absorption rate of randomly oriented magnetic nanoparticles in a static magnetic field

Ruslan A. Rytov<sup>1,2</sup>, Nikolai A. Usov<sup>2</sup>

<sup>1</sup>National University of Science and Technology «MISiS», Moscow, Russia

<sup>2</sup>Pushkov Institute of Terrestrial Magnetism, Ionosphere and Radio Wave Propagation, Russian Academy of Sciences, IZMIRAN, Troitsk, Moscow, Russia

## Abstract

The numerical simulation using the stochastic Landau-Lifshitz equation is performed to study magnetization dynamics of a dilute assembly of iron oxide nanoparticles subjected to a low-frequency alternating (ac) magnetic field with an amplitude  $H_{ac} = 200$  Oe and a frequency  $f = 300$  kHz and a static (dc) magnetic field in the range  $H_{dc} = 0 - 800$  Oe. The specific absorption rate of the assembly is calculated depending on the angle between the directions of the ac and dc magnetic fields. For the case of inhomogeneous dc magnetic field created by two opposite magnetic fluxes, the spatial distribution of SAR in the vicinity of the field-free point is obtained for assemblies with different nanoparticle size distributions. The results obtained seem to be helpful for the developing promising magnetic nanoparticle imaging and magnetic hyperthermia joint technique.

PACS: 75.20.-g; 75.50.Tt; 75.40.Mg

Keywords: Magnetic nanoparticles, Low frequency hysteresis loop, Specific absorption rate, Static magnetic field, Magnetic hyperthermia, Magnetic particle imaging

E-mail: ruslan.rytov@gmail.com (Ruslan A. Rytov, corresponding author)

## 1. Introduction

Magnetic nanoparticles, mainly iron oxides, are promising materials for the diagnosis and therapy of oncological diseases [1–3]. Important fields of application of magnetic nanoparticles in biomedicine are magnetic particle imaging (MPI) [4] and magnetic hyperthermia (MH) [1,2,5]. Magnetic hyperthermia uses the ability of magnetic nanoparticles to generate heat under the influence of an external alternating (ac) magnetic field of moderate frequency,  $f = 200\text{--}400$  kHz, and amplitude,  $H_{ac} = 100\text{--}200$  Oe [1,5,6]. In magnetic hyperthermia, magnetic nanoparticles are introduced into the tumor and heated by absorbing the energy of ac magnetic field. The intensity of heat release is characterized by the specific absorption rate (SAR) of an assembly. Maintaining in several medical treatments the distribution of temperature in the tumor in the range of  $41\text{--}43$  °C leads to the tumor destruction, as well as to the activation of the body's immune response to cancer cells [6]. However, the introduction of MH into clinical practice is hindered by a number of difficulties. Unfortunately, it is not easy to control the distribution of magnetic nanoparticles in the biological environment, as well as to monitor the temperature distribution in the heated area [1,2,6].

It is assumed [6–10] that some of these problems can be overcome by combining MPI and MH techniques. The MPI-MH combination will make it possible to monitor the distribution of nanoparticles in the living tissues during MH. In addition, by controlling the spatial distribution of the non-uniform dc magnetic field, it is possible to suppress SAR in the entire range of action of the ac magnetic field in the biological environment, except for a certain area near the free field point (FFP). This will allow localizing the heat release in the tumor area with millimeter accuracy. The search for optimal assemblies for joint MH-MPI therapy is an urgent task in this research area.

Experimental measurements of low-frequency hysteresis loops of assemblies under the influence of ac and dc magnetic fields were carried out in [11–12]. It was shown [11] that an application of dc magnetic field  $H_{dc} \geq 400$  Oe is sufficient to completely suppress the SAR of an assembly of FeCo nanoparticles. It was found also [12] that for magnetic nanoparticles in a liquid, an increase of the dc magnetic field leads to a decrease in the area of the hysteresis loop for both parallel and perpendicular configurations of external magnetic fields.

Analytical and numerical calculations of the dynamics of the nanoparticle magnetization in ac magnetic field in the presence of dc field were carried out in [13–19]. In particular, the behavior of assemblies of nanoparticles distributed in a viscous liquid was considered in [16–19]. However, nanoparticles in a liquid show more complex behavior due to the presence of both magnetic and mechanical degrees of freedom of the particles [15,20,21]. Meanwhile, in a biological environment, the rotation of magnetic nanoparticles as a whole under the action of ac

magnetic field is strongly hindered [22], so that the spatial orientation of nanoparticles in biological media can be considered fixed and random. In this case, the dynamics of the assembly magnetization depends on the parameters of the external magnetic field, as well as the magnetic and geometric parameters of an assembly [18,20,23,24].

To develop the joint MPI-MH technique, it is necessary to study in detail the dependence of the SAR of a randomly oriented assembly on the magnitude and direction of the external dc field with respect to that of the uniform ac field. In this work, using the numerical solution of the stochastic Landau-Lifshitz equation [15,18,20,21,24], the dynamics of non-interacting magnetic nanoparticles of iron oxide is considered in a wide range of particle diameters,  $D = 18 - 50$  nm. The SAR of the assembly is calculated depending on the amplitude and direction of the dc magnetic field in the range  $H_{dc} = 0 - 800$  Oe. The spatial distribution of the assembly SAR in the vicinity of the FFP has been obtained for the case of inhomogeneous dc magnetic field created by two opposite magnetic fluxes, for the case of assemblies with different nanoparticle size distributions.

## 2. Numerical simulation

Let us consider a dilute assembly of magnetic nanoparticles with uniaxial magnetic anisotropy randomly oriented in a solid matrix. The saturation magnetization of particles and the magnetic anisotropy constant are taken to be  $M_s = 350$  emu/cm<sup>3</sup> and  $K_1 = 10^5$  erg/cm<sup>3</sup>, respectively [25]. The range of nanoparticle diameters studied is  $D = 18 - 50$  nm, the temperature of the system is  $T = 300$  K. Let an assembly of nanoparticles be in ac magnetic field with an amplitude  $H_{ac} = 200$  Oe and a frequency  $f = 300$  kHz. These ac field parameters are typical for use in magnetic hyperthermia [1,5,6]. In this work, we are interested in the dependence of the assembly SAR on the intensity of dc external magnetic field, additionally applied to the assembly. It is assumed that the dc magnetic field varies in the range  $H_{dc} = 0 - 800$  Oe and is applied at different angles to the ac magnetic field direction. The behavior of a randomly oriented assembly under the combined action of ac and dc magnetic field is studied using numerical simulation based on the solution of the stochastic Landau-Lifshitz equation [15,18,20,21,24]. The SAR of a randomly oriented assembly is calculated in terms of the area of the low-frequency hysteresis loop according to the well-known formula [26, 27]

$$SAR = \frac{fM_s}{\rho} \oint \langle \vec{\alpha} \rangle d\vec{H}$$

where  $\rho$  is the density of the magnetic material,  $M_s \langle \vec{\alpha} \rangle$  is the average magnetization of an assembly of nanoparticles. To obtain statistically reliable results, low-frequency hysteresis loops are averaged over 30 independent realizations of randomly oriented assembly containing 60 non-interacting nanoparticles of a fixed diameter.

## 2a. $H_{dc}$ is parallel to $H_{ac}$

Let us first consider the case when external dc magnetic field in the range  $H_{dc} = 0 - 300$  Oe is applied parallel to the direction of the ac magnetic field with amplitude  $H_{ac} = 200$  Oe. The results of SAR calculation for a dilute, randomly oriented assembly depending on the value of the dc magnetic field are shown in Figure 1.

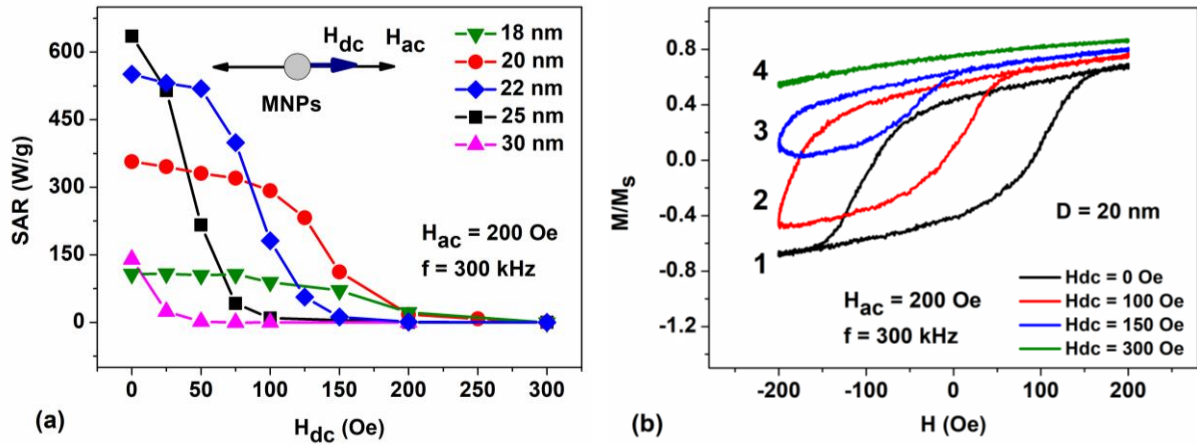


**Figure 1:** (a) Dependence of the SAR of randomly oriented assemblies of nanoparticles of various diameters distributed in a solid matrix on a dc magnetic field  $H_{dc}$  applied parallel to the ac field  $H_{ac}$ . (b) Low-frequency hysteresis loops for an assembly of nanoparticles with  $D = 20$  nm at different  $H_{dc}$  values: 1)  $H_{dc} = 0$ , 2)  $H_{dc} = 100$  Oe, 3)  $H_{dc} = 150$  Oe and 4)  $H_{dc} = 300$  Oe.

As Figure 1a shows, in the absence of dc magnetic field,  $H_{dc} = 0$ , there is an interval of optimal particle diameters,  $D = 18 - 30$  nm, where the SAR of the assembly exceeds 100 W/g at the given frequency and amplitude of the ac magnetic field. However, applying a dc magnetic field parallel to the ac field direction results in a significant SAR decrease. According to Figure 1a, to completely suppress the SAR of an assembly in a given field configuration, it is sufficient to fulfilled the inequality  $H_{dc} \geq H_{ac} = 200$  Oe, regardless of the particle diameters. However, the behavior of the function  $SAR(H_{dc})$  significantly depends on the nanoparticle diameter. For example, for particles with a diameter  $D < 22$  nm, the dc field in the range of  $H_{dc} < 100$  Oe has a relatively weak effect on the SAR, but then SAR decreases rapidly at  $H_{dc} > 100$  Oe. On the other hand, for particles with  $D = 25$  nm, which show the maximum SAR at  $H_{dc} = 0$ , even a relatively weak dc field,  $H_{dc} = 50$  Oe, causes a significant drop in the SAR of the assembly.

Figure 1b shows the change in the shape of the low-frequency hysteresis loop with increasing  $H_{dc}$  for a particular case of a randomly oriented assembly of nanoparticles with  $D = 20$  nm. It can be seen that the low-frequency hysteresis loop is strongly deformed as a function of  $H_{dc}$ . Namely, for positive values of the ac magnetic field, when the fields  $H_{ac}(t)$  and  $H_{dc}$  add up, the hysteresis loop of the assembly actually collapses. However, for negative values of  $H_{ac}(t)$ ,

when the ac and dc fields compensate each other, the loop area decreases significantly. Furthermore, with an increase in the amplitude of the dc field, the average magnetization of the assembly gradually increases, which leads in Figure 1b to an upward shift of the low-frequency hysteresis loop with increasing of  $H_{dc}$ . Finally, at  $H_{dc} \geq 300$  Oe the hysteresis loop collapses completely. Evidently, the absorption of the ac magnetic field energy in a sufficiently strong dc field is absent, since magnetization reversal of nanoparticles is impossible.

## 2b. $H_{dc}$ is perpendicular to $H_{ac}$

Let us now consider the case of perpendicular orientation of external dc and ac magnetic fields. The dc magnetic field changes in this case in the range  $H_{dc} = 0 - 800$  Oe. The results of SAR calculation as a function of  $H_{dc}$  for randomly oriented assemblies of nanoparticles with diameters  $D = 20 - 50$  nm are shown in Figure 2.

As Figure 2a shows, the SAR of assemblies of nanoparticles with  $D = 20$  and 25 nm rapidly decreases with increasing of  $H_{dc}$ . In fact, for particles of these diameters the SAR of the assembly is completely suppressed at  $H_{dc} \geq 300$  Oe. It is interesting to note, however, that, in contrast to the parallel field configuration, in the given case an interval of values  $H_{dc} = 100 - 300$  Oe appears, where the SAR of the assembly increases sharply for nanoparticles with  $D = 30 - 50$  nm. For example, as Figure 2a shows, for the assembly with  $D = 30$  nm, SAR rapidly increases at  $H_{dc} > 50$  Oe, reaches a maximum of 410 W/g at  $H_{dc} = 150$  Oe, and then gradually decreases with a further increase in  $H_{dc}$ . Complete suppression of the SAR for assemblies of particles with  $D = 30 - 50$  nm occurs in this case only at  $H_{dc} \geq 500$  Oe.

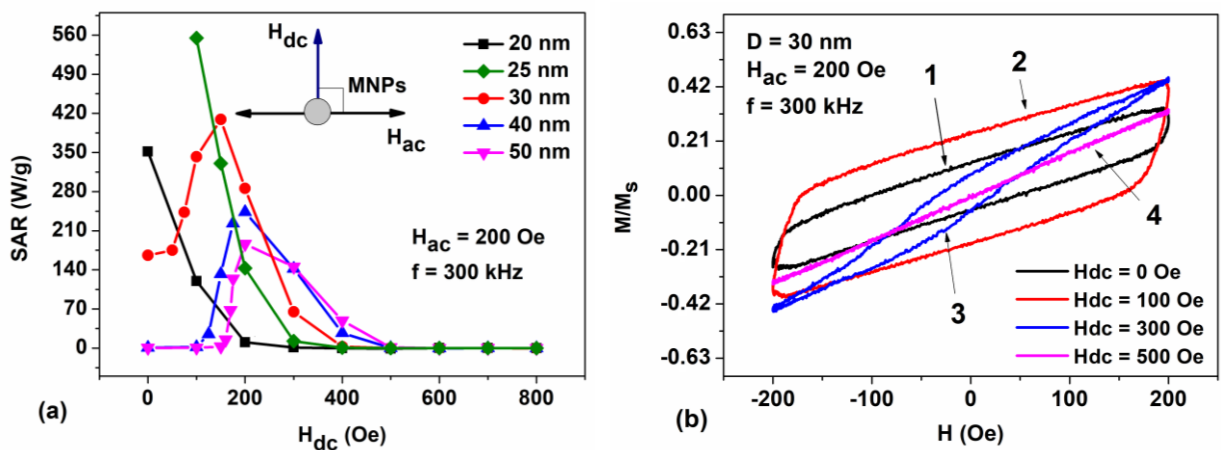


**Figure 2:** (a) Dependence of SAR on dc magnetic field applied perpendicular to ac magnetic field for randomly oriented assemblies of nanoparticles of various diameters. (b) Low-frequency hysteresis loops for an assembly of nanoparticles with  $D = 30$  nm as a function of  $H_{dc}$ : 1)  $H_{dc} = 0$ , 2)  $H_{dc} = 100$  Oe, 3)  $H_{dc} = 300$  Oe and 4)  $H_{dc} = 500$  Oe.

Figure 2b shows the shape of low-frequency hysteresis loops for nanoparticles with  $D = 30$  nm at different  $H_{dc}$  values. In the absence of dc field,  $H_{dc} = 0$ , the loop area is finite, and according to Figure 2a SAR of the assembly is 160 W/g. However, as the dc field increases to  $H_{dc} = 100$  Oe, the low-frequency hysteresis loop of the assembly expands and the SAR of the assembly increases to 350 W/g. However, with a further increase in  $H_{dc}$ , the area of the hysteresis loop gradually decreases, and, finally, the loop collapses completely at  $H_{dc} = 400$  Oe. The functions  $SAR(H_{dc})$  for a randomly oriented assembly of nanoparticles with diameters  $D = 40$  and 50 nm behave similarly.

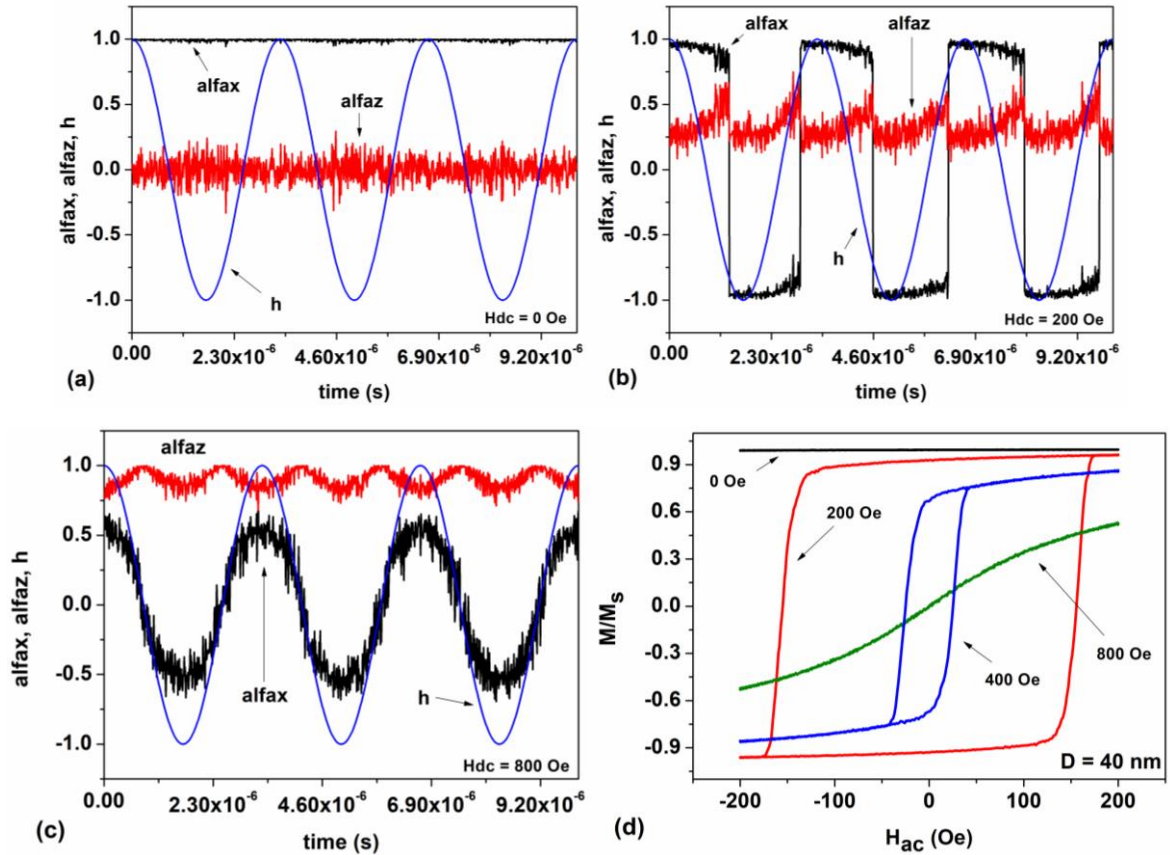


**Figure 3:** (a) Dynamics of  $\alpha_x$  and  $\alpha_z$  components of the unit magnetization vector of a nanoparticle with  $D = 30$  nm at  $H_{dc} = 0$ ;  $h$  marks the time dependence of the normalized ac magnetic field directed along the  $x$  axis. (b) The same in dc field  $H_{dc} = 200$  Oe directed along the  $z$  axis, perpendicular to the particle easy anisotropy axis. (c) The same for  $H_{dc} = 800$  Oe. (d) Low-frequency hysteresis loops of the nanoparticle for  $H_{dc} = 0, 200, 400,$  and  $800$  Oe, respectively.

To explain this effect, Figure 3 shows the magnetization dynamics of a nanoparticle with  $D = 30$  nm, with easy anisotropy axis parallel to the ac field direction. The latter is parallel to the  $x$  axis, whereas the dc magnetic field is assumed to be directed along the  $z$  axis (see inset in Figure 2a). Figures 3a – 3c show the dynamics of the  $\alpha_x$  and  $\alpha_z$  components of the particle unit

magnetization vector, as well as the time dependence of the normalized ac magnetic field, denoted by the symbol  $h$ . It is assumed that at the initial moment of time the unit magnetization vector of the particle is given by  $\alpha_x = 1$ . Irregular perturbations of the components of the unit magnetization vector occur due to thermal fluctuations of the particle magnetic moment at  $T = 300$  K.

As Figure 3a shows, in the absence of dc field,  $H_{dc} = 0$ , the unit magnetization vector of the particle fluctuates near the bottom of the potential well,  $\alpha_x \approx 1$ ,  $\alpha_z \approx 0$ . However, according to Figure 3b, as the dc field increases to  $H_{dc} = 200$  Oe, due to a change in particle energy barrier the  $\alpha_x$  component begins to jump between particle potential wells alternately taking values of  $\pm 1$ . Besides, at those times when the ac magnetic field is small,  $h \approx 0$ , the  $\alpha_z$  component rapidly increases and reaches the values  $\alpha_z \geq 0.5$ . As Figure 3d shows, at  $H_{dc} = 200$  Oe the low-frequency hysteresis loop of the particle becomes almost rectangular. As a result, the assembly SAR has a maximum at a given value of  $H_{dc}$ . With a further increase in  $H_{dc}$ , the dc field begins to dominate over the ac field, so that at  $H_{dc} = 800$  Oe the unit magnetization vector of the particle turns out to be mainly directed along the  $z$  axis, perpendicular to the ac magnetic field (see Figure 3c). As Figure 3d shows, this leads to a sharp drop in the particle hysteresis loop area.

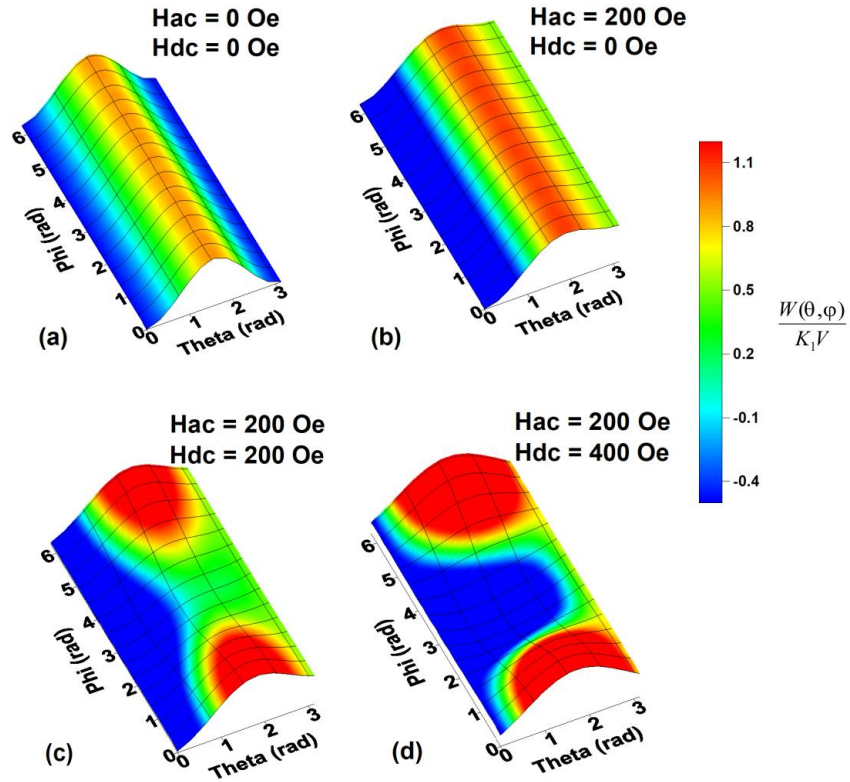


**Figure 4:** Evolution of the normalized energy density of the particle,  $W(\theta, \varphi)/K_1V$ , as a function of dc magnetic field applied perpendicular to the particle easy anisotropy axis: a) and b)  $H_{dc} = 0$  Oe, (c)  $H_{dc} = 200$  Oe and (d)  $H_{dc} = 400$  Oe.

In addition to Figure 3, Figure 4 shows the evolution of the surface of the normalized energy density of the nanoparticle,  $W(\theta, \varphi)/K_1V$ , as a function of the spherical angles  $\theta$  and  $\varphi$  in a dc magnetic field directed perpendicular to the particle easy anisotropy axis.

Figures 4a and 4b show the total energy of the particle in the absence of dc magnetic field,  $H_{dc} = 0$ , at times when the current ac magnetic field is zero or equal to its maximum value,  $H_{ac} = 200$  Oe, respectively. Obviously, at  $H_{dc} = 0$ , the potential wells of the nanoparticle located at  $\theta = 0$  and  $\theta = \pi$  are separated by a high potential barrier, which is independent of the  $\varphi$  angle. However, if perpendicular dc magnetic field increases to  $H_{dc} = 200$  Oe, a saddle trajectory appears on the barrier at  $\varphi = \pi$  (see Figure 4c). As a result, the height of energy barrier between the potential wells decreases significantly. This leads to an increase in the probability of magnetization reversal of nanoparticles of large diameters,  $D = 30\text{--}50$  nm. At  $H_{dc} = 200$  Oe this gives an almost rectangular hysteresis loop, shown in Figure 3d. However, in a sufficiently strong perpendicular magnetic field,  $H_{dc} = 400$  Oe, (Figure 4d), a deep potential well appears in which the magnetic moment of the particle is actually blocked,  $\alpha_x \approx 0$ ,  $\alpha_z \approx 1$ , since the direction of the dc magnetic field becomes energetically beneficial.

## 2c. Angle dependence of SAR

It is important to note that a saddle between potential wells also arises when a dc magnetic field is directed at some angle to the particle easy anisotropy axis. As a result, for particles of sufficiently large diameters,  $D = 30 - 50$  nm, oriented at a certain angle to the direction of dc magnetic field of sufficient magnitude, a significant decrease in the energy barriers occurs. It is these particles that make the main contribution to the increase in the assembly SAR with increasing  $H_{dc}$ , as Figure 2a shows. For smaller diameter particles,  $D < 25$  nm, a dc field only suppresses the SAR value, since the energy barriers for such particles are relatively small.

## 3. Application to MPI

With the joint implementation of the MPI-MH technique, the assembly of magnetic nanoparticles will be in a uniform ac magnetic field, as well as in a dc field with a complex spatial distribution. As shown above, a dc magnetic field is capable of both suppressing and increasing the SAR of an assembly, depending on the magnitude and relative orientation of the ac and dc magnetic fields, the characteristic diameter of magnetic nanoparticles being also important.

In this section, as an example of a possible SAR spatial distribution, we consider the situation when a polydisperse assembly of nanoparticles is in an inhomogeneous dc magnetic

field formed by two opposite magnetic fluxes. The assembly is excited by a uniform ac field created by Helmholtz coils. The SAR calculation is carried out in the vicinity of a corresponding FFP. The geometry of the system under consideration is schematically shown in Figure 5a.

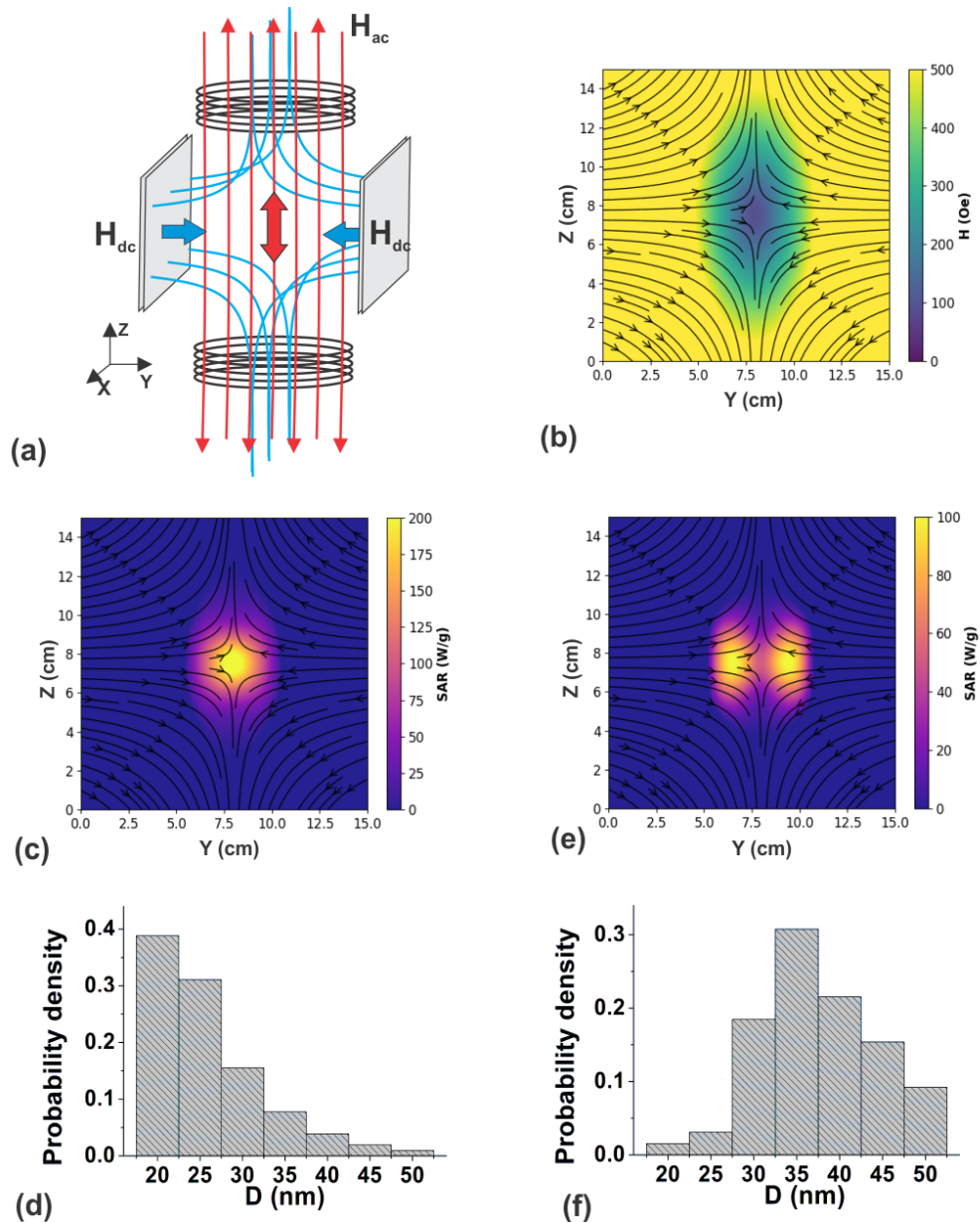


**Figure 5:** (a) Schematic representation of the crossed uniform ac and non-uniform dc magnetic field geometry with a FFP at the center of the system; (b) distribution of the amplitude and direction of the inhomogeneous dc field in the plane YZ, near the center of the system shown in Figure 5a; (c) SAR distribution in the vicinity of the FFP in the YZ plane for an assembly of fine nanoparticle fraction (d); (e) the same for coarse nanoparticle fraction (f).

Figure 5b shows the distribution of the magnitude and direction of a non-uniform dc magnetic field created by two opposite magnetic fluxes in the YZ plane in the vicinity of FFP.

The maximum value of the dc field outside the region under consideration is  $H_{dc} \sim 800$  Oe. However, it rapidly decreases to zero as the FFP is approached. A uniform ac magnetic field with amplitude  $H_{ac} = 200$  Oe and frequency  $f = 300$  kHz is directed along the Z axis. As Figure 5b shows, in the YZ plane the dc field direction turns out to be nearly perpendicular to the ac magnetic field in almost the entire region shown. Only near the center of the system, where the dc magnetic field is small, does it form a varying angle with the ac magnetic field direction.

Let the entire area shown in Figure 5b is filled with an immobile nonmagnetic medium containing a polydisperse assembly of randomly oriented magnetic nanoparticles. Let us first consider an assembly predominantly consisting of nanoparticles with  $D < 25$  nm. The results of the calculation of local SAR values for this assembly in the geometry of dc magnetic field, shown in Figure 5b, are presented in Figure 5c. The particle size distribution for this assembly is given in Figure 5d. It is easy to see that in the given case only particles located in a small cylindrical region near the FFP with a radius of about 1 cm are capable of effectively absorbing the energy of the ac magnetic field. Furthermore, near the FFP the assembly SAR reaches 200 W/g.

However, if the assembly of nanoparticles contains a large fraction of nanoparticles, with the particle size distribution shown in Figure 5f, the spatial SAR distribution near the FFP changes. Figure 5e shows that in this case the SAR of the polydisperse assembly does not exceed 100 W/g and, is nonzero in a bagel structure with a radius of about 2 cm, centered at the FFP. It is important to note also that in this case, near the FFP point itself, the SAR is minimal, since the presence of a sufficiently strong dc magnetic field is necessary to activate the fraction of big magnetic nanoparticles.

The above example shows that in order to implement the combined MPI-MH method, it is necessary to first calculate the local distribution of SAR in the biological environment, taking into account the geometry and magnitude of dc and ac magnetic fields, as well as the size distribution in an assembly of magnetic nanoparticles. In particular, in the considered example, it seems preferable to use an assembly of nanoparticles with a narrow size distribution in the range  $D = 20\text{--}25$  nm.

#### 4. Conclusions

It is known [1,2,5] that optimized assemblies of magnetic nanoparticles are promising for use in magnetic hyperthermia. However, it is necessary to strictly control the spatial distribution of magnetic nanoparticles in the tumor in order to exclude undesirable thermal effects on healthy tissues surrounding the tumor [28]. The combination of MH-MPI techniques seems promising, as it will allow localizing the heat release in the tumor-affected organ more accurately and

minimizing the thermal effect on healthy tissues, which may also contain a certain amount of magnetic nanoparticles. Obviously, to implement this approach, it is necessary to study the thermal capacity of the assembly distributed in a biological medium under simultaneous action of uniform ac and inhomogeneous dc field, depending on the field geometry, the magnetic parameters of the nanoparticles, and their characteristic sizes.

In this paper, numerical simulation of the stochastic Landau-Lifshitz equation is used to study the dynamics of magnetization in a dilute, randomly oriented assembly of iron oxide nanoparticles under the combined action of ac and dc magnetic fields. It is shown that for nanoparticles with a diameter  $D < 25$  nm, the SAR of the assembly monotonically decreases with increasing  $H_{dc}$ , regardless of the angle between the ac and dc fields. Complete suppression of SAR in this case occurs at  $H_{dc} \geq H_{ac}$ . Therefore, iron oxide nanoparticles with diameters  $D = 20 - 25$  nm seem preferable for use in MPI-MH combined therapy, since in this case the maximum heat release is concentrated in a well-localized region near the FFP.

On the other hand, it is found that for nanoparticles of larger diameters,  $D \geq 30$  nm, the change in the assembly SAR with an increase in the dc magnetic field has a nonmonotonic character. Namely, in the range  $H_{dc} = 100 - 300$  Oe the SAR of randomly oriented assembly can increase appreciably, since a dc magnetic field significantly lowers the energy barriers between potential wells for nanoparticles whose easy axes are oriented at finite angles to the dc field direction. As a result, for larger nanoparticles,  $D > 30$  nm, a significant decrease in SAR can occur near the FFP, where the dc field is low, since the magnetization reversal of large particles in this region is prohibited.

### **Acknowledgment**

R. A. Rytov gratefully acknowledges the financial support of the Ministry of Science and Higher Education of the Russian Federation in the framework of Increase Competitiveness Program of NUST «MISIS», contract № K2A-2019-034.

### **References**

1. Périgo, E. A.; Hemery, G.; Sandre, O.; Ortega, D.; Garaio, E.; Plazaola, F.; Teran, F. J. *Appl. Phys. Rev.* **2015**, 2, 041302.
2. Pankhurst, Q. A.; Thanh, N. T. K.; Jones, S. K.; Dobson, J. *J. Phys. D: Appl. Phys.* **2009**, 42, 224001.
3. Gloag, L.; Mehdipour, M.; Chen, D.; Tilley, R. D.; Gooding, J. J. *Adv. Mat.* **2019**, 31, 1904385.
4. Gleich, B.; Weizenecker, J. *Nature* **2005**, 435, 1214–1217.

5. Rodrigues, H. F.; Capistrano, G.; Bakuzis, A. F. *Int. J. Hyp.* **2020**, *37*, 76–99.
6. Lu, Y.; Rivera-Rodriguez, A.; Tay, Z. W.; Hensley, D.; Fung, K. L. B.; Colson, C.; Saayujya, C.; Huynh, Q.; Kabuli, L.; Fellows, B.; et al. *Int. J. Hyp.* **2020**, *37*, 141–154.
7. Chandrasekharan, P.; Tay, Z. W.; Hensley, D.; Zhou, X. Y.; Fung, B. K.; Colson, C.; Lu, Y.; Fellows, B. D.; Huynh, Q.; Saayujya, C.; et al. *Theranostics* **2020**, *10*, 2965–2981.
8. Myrovali, E.; Maniotis, N.; Samaras, T.; Angelakeris, M. *Nanoscale Adv.* **2020**, *2*, 408–416.
9. Bauer, L. M.; Situ, S. F.; Griswold, M. A.; Samia, A. C. S. *Nanoscale* **2016**, *8*, 12162–12169.
10. Dadfar, S. M.; Camozzi, D.; Darguzyte, M.; Roemhild, K.; Varvarà, P.; Metselaar, J.; Banala, S.; Straub, M.; Güvener, N.; Engelmann, U.; et al. *J. Nanobiotech.* **2020**, *18*.
11. Mehdaoui, B.; Carrey, J.; Stadler, M.; Cornejo, A.; Nayral, C.; Delpech, F.; Chaudret, B.; Respaud, M. *Appl. Phys. Lett.* **2012**, *100*, 052403.
12. Onodera, R.; Kita, E.; Kishimoto, M.; Kuroiwa, T.; Yanagihara, H. *IEEE Trans. on Magn.* **2021**, *57*, 1–5.
13. Ota, S.; Matsugi, Y.; Nakamura, T.; Takeda, R.; Takemura, Y.; Kato, I.; Nohara, S.; Sasayama, T.; Yoshida, T.; Enpuku, K. *J. Magn. Magn. Mat.* **2019**, *474*, 311–318.
14. Déjardin, P. M.; Kalmykov, Yu. P.; Kashevsky, B. E.; El Mrabti, H.; Poperechny, I. S.; Raikher, Yu. L.; Titov, S. V. *J. Appl. Phys.* **2010**, *107*, 073914.
15. Shasha, C.; Krishnan, K. M. *Adv. Mat.* **2020**, *33*, 1904131.
16. Murase, K. *Open J. Appl. Sci.* **2016**, *06*, 839–851.
17. Zhao, Z.; Rinaldi, C. *The J. Phys. Chem. C*, **2018**, *122*, 21018–21030.
18. Engelmann, U. M.; Shasha, C.; Teeman, E.; Slabu, I.; Krishnan, K. M. *J. Magn. Magn. Mat.* **2019**, *471*, 450–456.
19. Dhavalikar, R.; Rinaldi, C. *J. Magn. Magn. Mat.* **2016**, *419*, 267–273.
20. Usov, N. A.; Liubimov, B. Ya. *J. Appl. Phys.* **2012**, *112*, 023901.
21. Usov, N. A.; Rytov, R. A.; Bautin, V. A. *Sci. Rep.* **2021**, *11*.
22. Soukup, D.; Moise, S.; Céspedes, E.; Dobson, J.; Telling, N. D. *ACS Nano*, **2015**, *9*, 231–240.
23. Yoshida, T.; Matsugi, Y.; Tsujimura, N.; Sasayama, T.; Enpuku, K.; Viereck, T.; Schilling, M.; Ludwig, F. *J. Magn. Magn. Mat.* **2017**, *427*, 162–167.
24. Usov, N. A.; Nesmeyanov, M. S.; Gubanova, E. M.; Epshtein, N. B. *B. J. Nano.* **2019**, *10*, 305–314.
25. Chikazumi, S. *Physics of Magnetism*; Wiley, New York, 1964.
26. Rosensweig, R. E. *J. Magn. Magn. Mat.* **2002**, *252*, 370–374.
27. Usov, N. A. *J. Appl. Phys.* **2010**, *107*, 123909.
28. Rytov, R. A.; Bautin, V. A.; Usov, N. A. *Sci. Rep.* **2022**, *12*.